Modeling Earth Systems and Environment (2020) 6:139–149
https://doi.org/10.1007/s40808-019-00666-z

ORIGINAL ARTICLE

An effective approach for the adsorptive removal of lead from an aqueous medium using nano *Prosopis Cineraria* leaf ash (NPCLA): characterization, operational effects, and recyclability

Arash Afsar Shahmaleki[1] · Mohsen Motevassel[1] · Ali Akbar Isari[2] · Bagher Anvaripour[1]

Received: 20 July 2019 / Accepted: 12 October 2019 / Published online: 2 November 2019

Abstract
Currently, the pollution of water by heavy metals is a common environmental problem because heavy metals are non-biodegradable and dangerous to human health at very low concentrations. Lead is one of the most prevalent heavy metals utilized in various industrial processes. In this study, an adsorbent made from nano *Prosopis cineraria* leaf ash (NPCLA) was successfully synthesized and characterized for the first time using Brunauer–Emmett–Teller (BET) method, field emission scanning electron microscope (FESEM), Fourier-transform infrared spectroscopy (FTIR), X-ray diffraction (*XRD*), energy-dispersive spectroscopy (EDS), and energy-dispersive analysis of X-rays (EDAX). The findings from the XRD analysis showed that the structure of the NPCLA predominantly included $CaCO_3$ and SiO_2 crystal phases. Batch adsorption experiments were performed as a function of reaction time, pH (2–10), initial concentration of lead (30–120 mg/L), and NPCLA dosage (1–3 g/L). According to the results, the lead ions were completely removed from an aqueous solution at a temperature of 25 °C with an NPCLA dosage of 2.5 g/L, an initial lead concentration of 30 mg/L, pH of 6, and after 100 min of reaction time. The NPCLA adsorbent demonstrated high stability and recyclability after six runs of the lead removal experiments. The equilibrium adsorption data were fitted to a pseudo-second-order kinetic model and the Langmuir isotherm model.

Keywords Nano adsorbent · Lead removal · Operational effects · Characterization

Introduction

Due to rapid industrial development, the amount of discharge of metal wastes has increased over the past few years. The pollution of water resources has also become a global concern because much of the wastewater discharged into natural water channels contains heavy metals. Heavy metals can be toxic at low concentrations (0.1–10 mg/L) and can also have lethal effects on human health and the environment, which can be irreparable (Nadeem et al. 2006; Wang and Chen 2006). Unlike the majority of organic pollutants, which easily biodegrade into harmless end products, heavy metals are non-biodegradable (El-Ashtoukhy et al. 2008; Zamani et al. 2013). Metals that are harmful to humans and ecological environments include cadmium (Cd), lead (Pb), copper (Cu), manganese (Mn), chromium (Cr), arsenic (As), mercury (Hg), and tin (Sn). Some metals can be assimilated and stored in the body and cause harmful diseases, such as cancers and accumulative poisoning (Nadeem et al. 2006; Li et al. 2002). Lead is a common contaminant of industrial wastewaters from many process industries including the manufacture of printing inks, storage, batteries, dyes, insecticides, paints, beverages, pigments, and leaded glass (Gueu et al. 2007; Günay et al. 2007; Wang et al. 2007). Lead can damage the liver, kidney, cardiovascular system, reproductive system, and nervous system. Symptoms of lead poisoning include insomnia, anemia, dizziness, tremors, cognitive

✉ Mohsen Motevassel
motavassel@put.ac.ir

Arash Afsar Shahmaleki
arash.afsh@yahoo.com

Ali Akbar Isari
aliichemeng@gmail.com

Bagher Anvaripour
anvaripour@put.ac.ir

[1] Department of Chemical Engineering, Abadan Faculty of Petroleum Engineering, Petroleum University of Technology, Abadan, Iran

[2] Department of Basic and Applied Sciences for Engineering, SAPIENZA University of Rome, Rome, Italy

deficits, convulsions, and hallucinations. The World Health Organization (WHO) has established a maximum concentration of 0.05 mg/L lead in drinking water, while the Environmental Protection Agency (EPA) has determined the action level to be 0.015 mg/L (Bachari et al 2019; Ozdes et al. 2009). Therefore, there is a need to develop effective operational methods to remove lead from water to meet the acceptable levels (Payan et al. 2019).

Different methods have been suggested for the removal of heavy metals including electrochemical precipitation, chemical precipitation, evaporation, coagulation, reverse osmosis, ion exchange, membrane separation, and adsorption. However, there are disadvantages and also limitations associated with these methods such as high energy consumption, difficult disposal of sludge, low selectivity, and high capital and operational costs. In addition, these methods can be effective in removing heavy metals at high concentrations and they also become inefficient at low concentrations. For example, electrochemical and chemical precipitation treatments are not effective at low (1–100 mg/L) concentrations of metal ions. Furthermore, treatment methods produce secondary wastes, which need to be treated in huge settling tanks. There is a significant cost associated with the ion exchange technique, while there are many problems related to adsorption by activated carbon, such as adsorbent regeneration and contaminant recovery (Bhattacharyya and Sharma 2004; Wang and Chen 2006; Chakravarty et al. 2010; Dubey and Shiwani 2012; Hafshejani et al. 2015). The adsorption technique has been introduced as the most effective method because of its high removal efficiency, accessibility to various adsorbents, economic operating cost, easy handling, as well as low impact on the environment (Ozdes et al. 2009; King et al. 2007; Bhatnagar and Sillanpää 2010; Okoye et al. 2010).

In recent years, nanotechnology applications have been used to treat polluted water and remove various contaminants. Because of their large surface area and high porosity, nanoparticles have the potential to be used as adsorbing substances (Liu and Zhang 2007; Hafshejani et al. 2015). According to the related literature, there are several biological and natural adsorbents including seaweed, olive stones, peanut hulls, neem bark, cocoa shells, chitin beads, orange peels, tea waste, grape stalks, coffee residue, cactus leaves, bael leaves, rice husks, pine leaves, bagasse waste, coconut copra, nut shells, tree ferns, and maize leaves (Bhattacharyya and Sharma 2004; Chakravarty et al. 2010; Mondal 2009; Naiya et al. 2009; Qaiser et al. 2009; Dizadji et al. 2011). In this respect, *Prosopis cineraria* is a member of the pea family adapted to live in semi-arid and arid regions. It is also known as one of the most important native tree species in Saudi Arabia, Yemen, UAE, Oman, Iran, Pakistan, and India. This plant has been often used for soil stabilization, livestock feeding, as a source of wood and firewood, and for therapeutic applications such as treating vertigo, dyspnea, cough, asthma, rheumatism, and skin diseases. Various studies have also reported that it can be employed as an adsorbent (Kaushik and Kumar 2003; Manikandar et al. 2009; Garg and Mittal 2013; Eshraghi et al. 2016; Malakootian et al. 2017; Pourjaafar 2017).

In the present study, NPCLA was synthesized in a one-pot method and used as a novel adsorbent for lead in aqueous solutions. The properties of the NPCLA was determined using XRD, FESEM, BET, FTIR, EDAX, and EDS techniques. Batch adsorption experiments were used to determine the adsorption efficiency of NPCLA as a function of solution pH, NPCLA dosage, initial lead concentration, and contact time. Furthermore, the stability of NPCLA during the experiments was investigated. Finally, the adsorption kinetics and isotherms of lead on the NPCLA surface were studied.

Materials and methods

Materials

All of the chemical reagents were purchased from Merck & Co. Inc. Double-distilled water was used in the stock solutions and no extra treatment was provided.

NPCLA synthesis

The *Prosopis cineraria* leaves were collected in Abadan, Iran. At first, the leaves were washed thoroughly with double-distilled water to eliminate any impurities. Then, they were heated in an electric oven at 105 °C for 1 day and subsequently calcined in a muffle furnace at 500 °C for 10 h. Next, the leaves were ground using a mechanical grinder. The powder was also sieved to produce the 53–75 µm fractions. Afterward, the powder was rewashed using deionized water and 0.001 MHCl to remove any remaining precipitated salt. Finally, the powder was heated in an electric oven at 80 °C overnight.

Characterization tests

The specific surface areas of the NPCLA were analyzed using the N_2 adsorption/desorption isotherms at 77 K on a BELSORP-miniII (Bel, Japan) adsorption apparatus. The morphology of the adsorbent and the size of the particles were also evaluated using FESEM MIRA3 microscope instrument (TECSAN, Czech Republic). The functional groups and bonds in the NPCLA were subsequently determined via FTIR spectroscopy as recorded on a VERTEX 70 spectrometer (Bruker, Germany). To assess the structural features of the NPCLA, XRD analysis was conducted on a PW1730 X-ray diffractometer (Philips, Netherlands) equipped with a Cu

anode (λ = 1.5406 Å) as an extinction source. A flame atomic absorption spectrometer (FAAS) (Jena, Germany) was finally employed to determine the lead concentration.

Adsorption experiments

In this study, $Pb(NO_3)_2$ (M_W = 331.1998 g/mol, Merck) was dissolved in deionized water to prepare the lead solutions; 0.2 M NaOH or HCl was used to adjust the pH of the solutions. Batch absorption studies were conducted in 100 mL bath reactors. Specific doses of NPCLA (1 g/L, 1.5 g/L, 2 g/L, 2.5 g/L, and 3 g/L) were added to the mixture and the flasks were put on a mechanical shaker at 250 rpm for 1 h. To obtain the final concentration of lead, 10 mL of the solution was centrifuged using the universal PIT 320 centrifuge (Iran) for 15 min at 15,000 rpm to remove any remaining adsorbent in the sample. The amount of adsorbed lead was determined using the FAAS to calculate the removal rate of lead. Note that all the runs were conducted at an ambient temperature of 25 °C. The percentage of lead removal was calculated using Eq. (1):

$$\text{Pb(II)removal}(\%) = \left(C_i - C_e\right) / C_i \times 100, \tag{1}$$

where C_e and C_i are the final and initial concentrations of lead, respectively.

The adsorption capacity of the system was obtained using Eq. (2):

$$q_e = \left(C_{t0} - C_e\right) \times \frac{V}{M_c} \tag{2}$$

where C_{t0} is the initial lead concentration (mg/L), C_e is the concentration of lead at the adsorption equilibrium state (mg/L), V is the volume of the mixture (L), and M_c is the weight of the NPCLA (g).

Theory

Adsorption isotherm

The adsorption isotherm describes the equilibrium between molecules absorbed by absorbent and remained in the solution. In this article, Freundlich and Langmuir isotherms were used to model the adsorption of Pb(II) on NPCLA.

Langmuir isotherm

The Langmuir isotherm is based on the assumption of monolayer molecule adsorption on finite sites of the adsorbent surface with uniform energy distribution. It is given by Eq. (3):

$$\frac{C_e}{q_e} = \frac{1}{K_L q_m} + \frac{C_e}{q_m}, \tag{3}$$

where q_e is the metal amount that the adsorbent adsorbed (mg/g), K_L and q_m are Langmuir constants related to the adsorption energy (L/g) and capacity (mg/g).

Freundlich isotherm

The Freundlich isotherm relies on non-uniform energy distribution of adsorption on a heterogeneous surface and is proportional to both mono- and multilayer adsorption. The linear form of Freundlich isotherm is represented by Eq. (4):

$$\log q_e = \log K_f + \frac{1}{n} \log C_e \tag{4}$$

where q_e is the equilibrium concentration of the solid phase, C_e is the equilibrium concentration of the liquid phase and n and K_f are Freundlich constant adsorption capacity and adsorption intensity, respectively.

Adsorption kinetic

In this article, to predict the mechanism of Pb(II) adsorption on NPCLA, pseudo-first-order and second-order kinetics were studied.

Pseudo-first-order kinetic

The pseudo-first-order represents the sorption capacity of solids in the liquid–solid system. This model describes the sorption of one lead ion onto one NPCLA sorption site:

$$A + \text{Pb}_{aq}^{+2} \longrightarrow k_1 A\text{Pb}_{\text{solid phase}} \tag{5}$$

where A is a vacant sorption site on the NPCLA and k_1 is the reaction rate constant.

The linear form of pseudo-first order is represented by Eq. (6):

$$\log\left(q_e - q_t\right) = \log q_e - \left(\frac{k_1}{2.303}\right) t, \tag{6}$$

where q_t and q_e are the capacities of adsorption at time t and equilibrium. By drawing $\log\left(q_e - q_t\right)$ versus t, q_e and k_1 are achieved.

Pseudo-second-order kinetic

The pseudo-second-order equation is modeled to studying chemisorption kinetics from liquid solutions. The linear form of pseudo-second order is represented by Eq. (7):

$$\frac{1}{q_e - q_t} = \frac{1}{q_e} + k_2 t, \tag{7}$$

where k_2 is the reaction rate constant and by drawing $\frac{1}{q_e - q_t}$ versus t, q_e and k_2 are achieved.

It assumes the sorption of one lead ion onto two NPCLA sorption sites:

$$2A + \mathrm{Pb}^{+2}_{\mathrm{sol}} \longrightarrow k_2 A^2 \mathrm{Pb}_{\text{solid phase}}. \quad (8)$$

Intraparticle diffusion

The intraparticle diffusion model assumes that this model is the only rate-controlling step and film diffusion is negligible. According to the Weber–Morris model, the intraparticle diffusion is represented by Eq. (9):

$$q_t = K_{\mathrm{id}} t^{0.5} + C, \quad (9)$$

where q_t are the capacities of adsorption at time t and K_{id} is the rate constant of the intraparticle diffusion and can be achieved by plotting q_t versus $t_{0.5}$.

Result and discussion

Characterization of NPCLA

BET

Figure 1a, b shows the N_2 adsorption/desorption isotherms of NPCLA and the Barrett, Joyner, and Halenda (BJH) pore size distribution of the NPCLA adsorbent, respectively. As can be seen in Fig. 1a, the NPCLA was identified as a type III isotherm with an overlap of the H_2 hysteresis loop at relative pressure in the range of 0.77–0.98, which demonstrated that the adsorbent had a mesostructured nature with dominant slit-shaped pores. The specific surface area (S_a) of the NPCLA was found to be 10.9 m^2/g. As shown in Fig. 1b, the major pore diameter distributions of the specimens were found in the range of 8–25 nm, which categorized the material as mesoporous according to the International Union of Pure and Applied Chemistry (IUPAC); these results were in excellent accordance with the obtained results about hysteresis loops discussed in a previous study (Isari et al. 2018). The results from the BET analysis indicated that the prepared NPCLA had a mesoporous structure and, thus, could be used as an effective adsorbent due to its high specific surface area and pore structure.

XRD

XRD is used to determine the properties of the crystallographic structures and the possible chemical composition of the samples (Hayati et al. 2018). For the XRD analysis in this study, the NPCLA was ground and homogenized. The XRD data of the NPCLA are shown in Fig. 2. According to the JCPDS numbers 00-047-1518 and 01-086-0174, the obtained peaks were attributed to the existence of $CaCO_3$ and $CaSi_2$ phase crystal structures (Bux et al. 2010; Oh et al. 2014). Furthermore, the grain size of the NPCLA was determined using the Scherrer equation from the broadening peak of NPCLA at 28.12° and was found to be 11.12 nm.

FTIR

FTIR spectroscopy was studied to investigate the bonds formed in the as-synthesized absorbent. Figure 3 illustrates that all the peaks occurred in the region of 400–4000 cm^{-1}.

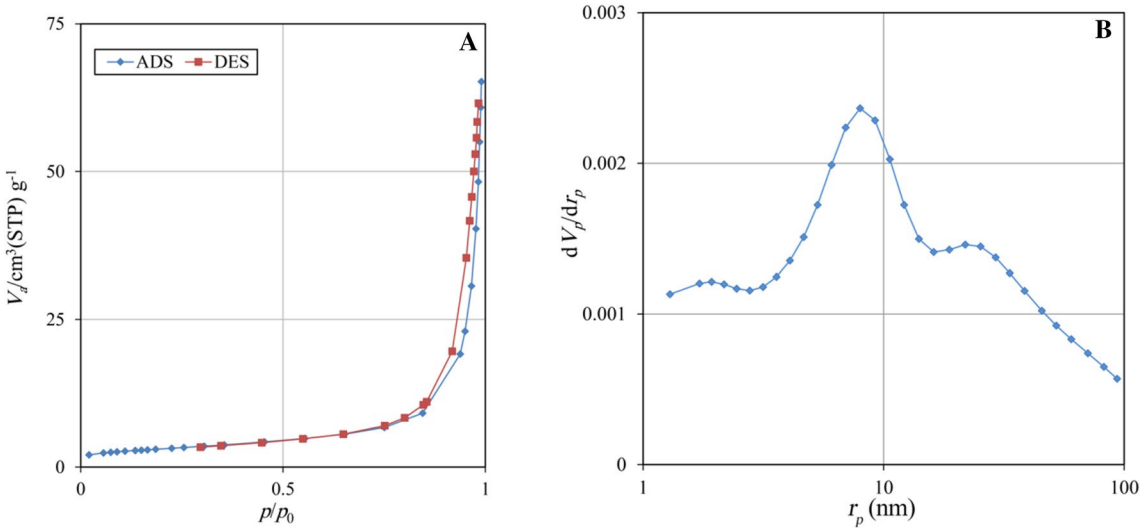

Fig. 1 **a** The N_2 adsorption/desorption isotherms of NPCLA and **b** the BJH pore size distribution of NPCLA

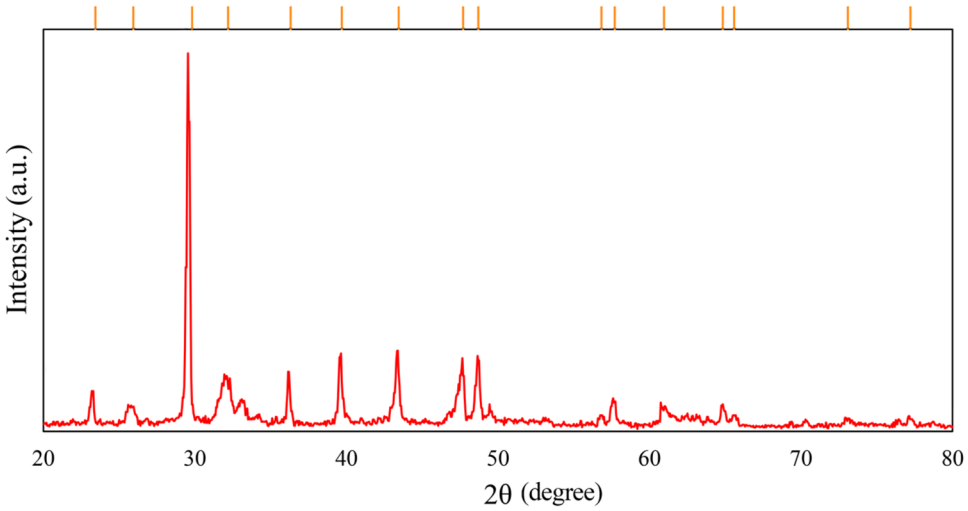

Fig. 2 The XRD pattern of the NPCLA absorbent

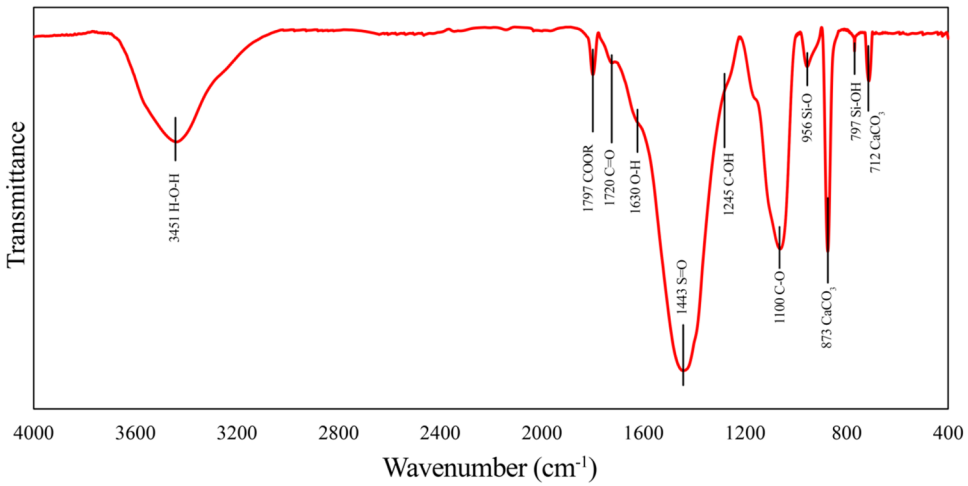

Fig. 3 FTIR spectrum of NPCLA

The FTIR pattern of the as-synthesized NPCLA revealed there was a small shoulder at 1630 cm^{-1}, which corresponded to water deformation vibration, and a broad band in the range of 3358–3562 cm^{-1}, which corresponded to the stretching vibrations of water and the hydroxyl groups (Pouretedal and Sadegh 2014). The main functional groups of the NPCLA were at 1100 cm^{-1}, 1245 cm^{-1}, 1443 cm^{-1}, 1720 cm^{-1}, and 1797 cm^{-1}, which corresponded to the C–O stretching vibration, C–OH stretching peak, S=O stretching vibration, C=O stretching vibration, and carboxylate stretching vibration, respectively (Granbohm et al. 2017). The bands at 712 cm^{-1} and 873 cm^{-1} were fingerprints of $CaCO_3$, which were shown in the XRD analysis (Ramasamy et al. 2017). In addition, the small peaks at 797 cm^{-1} and 956 cm^{-1} related to the presence of SiO_2, which showed the Si–O–H and Si–O bonds, respectively (Tang et al. 2008; Gholipour et al. 2012; Dippong et al. 2017).

FESEM

The FESEM micrographs of NPCLA are shown in Fig. 4. The micrographs indicate that the nanoparticles had an agglomerated spherical-shaped morphology. The average particle size of the NPCLA was 30–40 nm. It must be noted that there was a small discrepancy between the measured size using the Scherrer formula and the size determined from the FESEM images, which could be attributed to the small agglomerations of the nanoparticles during the synthesis of the NPCLA (Isari et al. 2018).

EDAX and EDS dot mapping

The EDAX and EDS are methods used for studying the element compositions in nanoparticles (Ponce-Lira et al. 2017). Figure 5 presents the EDAX results of the NPCLA. The main elements in the adsorbent were C, Ca, O, and Si; other peaks in the EDAX data corresponding to various elements

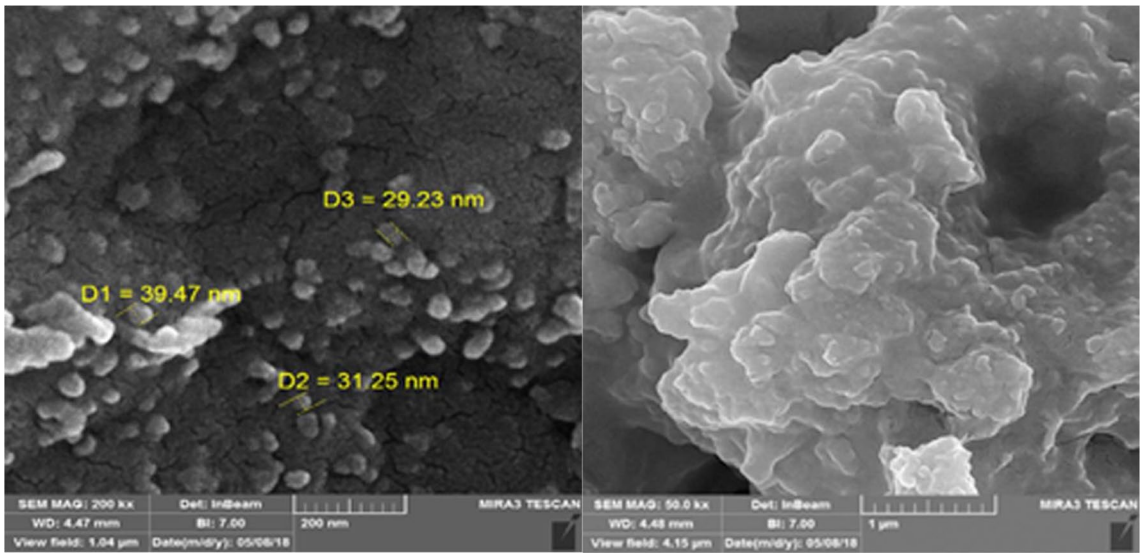

Fig. 4 FESEM micrographs of NPCLA

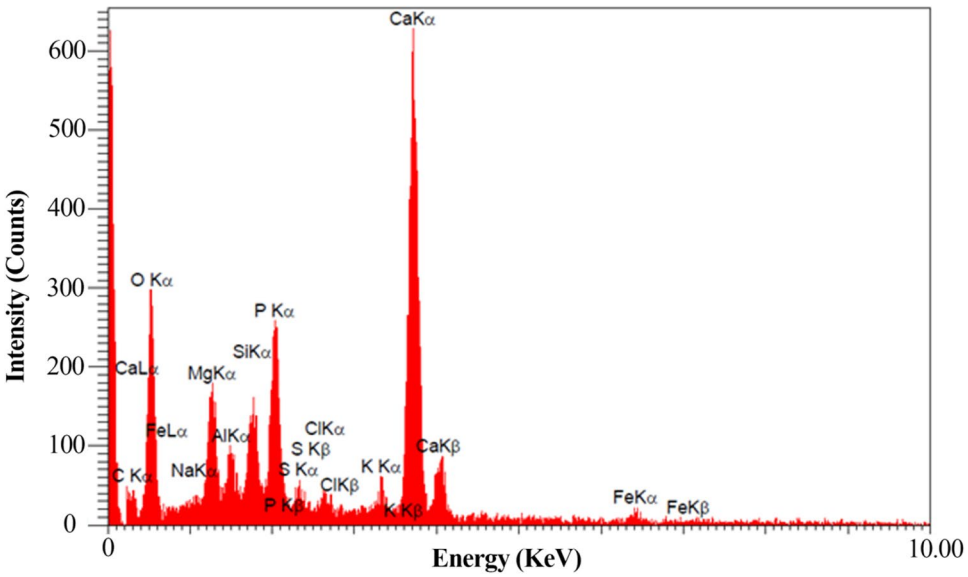

Fig. 5 EDAX elemental composition of NPCLA

indicated that ashes and contaminates remained even after the washing process during the synthesis step. Figure 6a–e shows the EDS dot mapping for the NPCLA adsorbent. The figures show that the elements had a uniform distribution over the NPCLA surface. As a result, it was concluded that the fabricated particles had highly porous structures that could be sufficient for the adsorption process.

Adsorbent performance

Effect of pH

The pH of the initial mixture is known as one of the most important factors influencing the adsorptive process. In this study, pH changes ranging from 2 to 10 were studied. The effect of pH on the adsorption of lead via NPCLA is shown in Fig. 7. The results revealed that the removal efficiency had gradually improved as the pH increased from 2 to 6. However, as the pH had went up from 6 to 10, the removal efficiency decreased. At low pH values, the H^+ ions had competed with the lead ions for the active and free sites on the NPCLA surface, since the concentration of H^+ ions in an aqueous medium was reported to be high. As the pH value had increased, the concentration of H^+ ions had reduced; thus, competition for the sites had also decreased (Chakravarty et al. 2010). Given that the negative charges on the adsorbent surface had increased as the pH value was added, a rising trend could be observed in lead adsorption

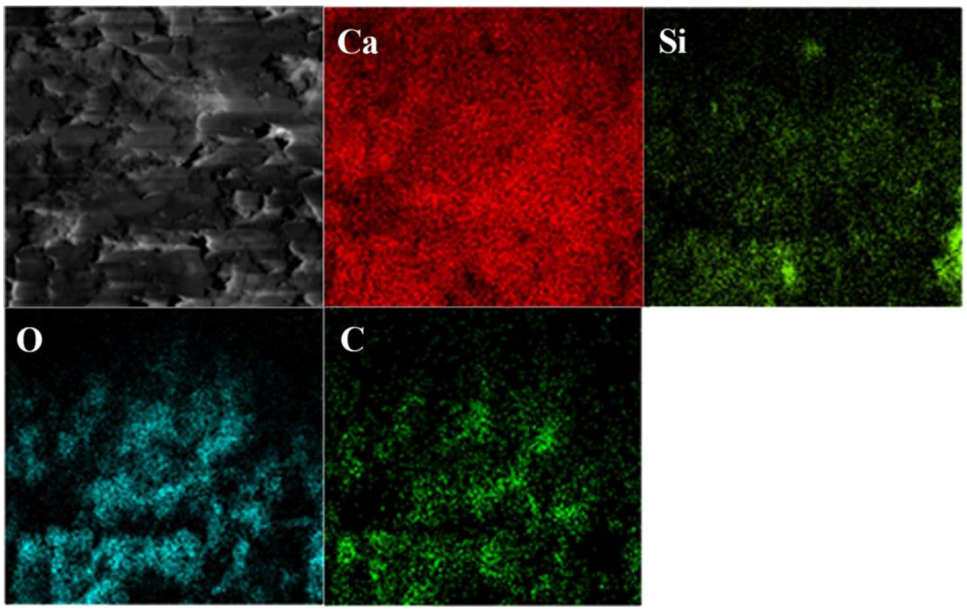

Fig. 6 EDS dot mapping of NPCLA: (a) overall, (Ca) calcium, (Si) silicon, (O) oxygen, and (C) carbon

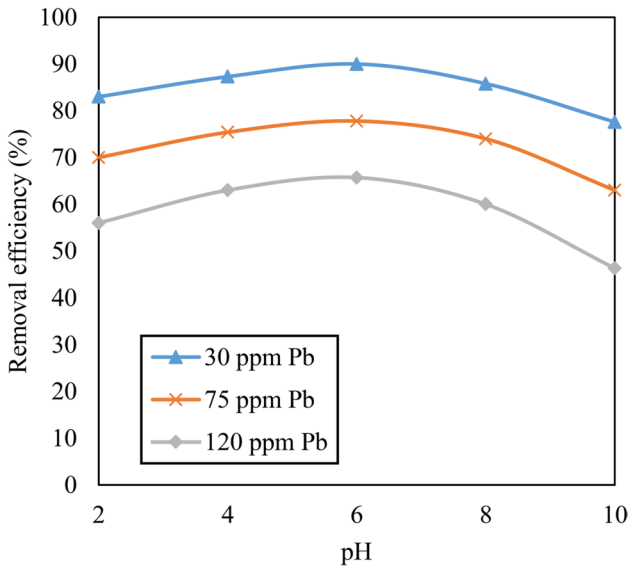

Fig. 7 Effect of pH on the adsorption of 30 ppm lead, 75 ppm lead, and 120 ppm lead by 1.5 g/L NPCLA at a temperature of 25 °C

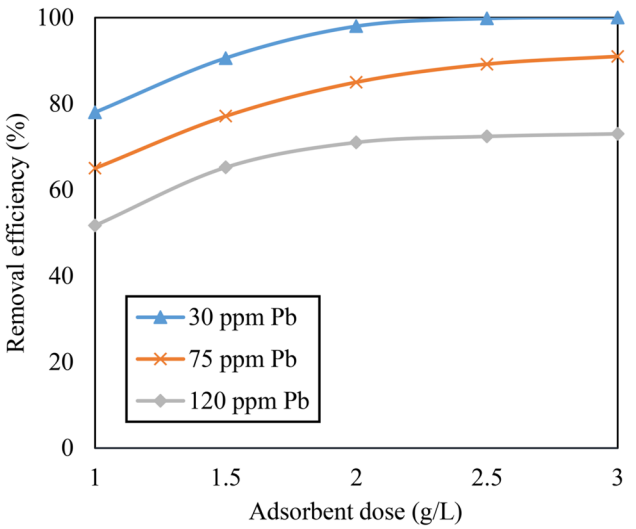

Fig. 8 Effect of adsorbent dose on lead adsorption by NPCLA at 30 ppm lead, 75 ppm lead, and 120 ppm lead, pH of 6, and a temperature of 25 °C

by NPCLA. The decrease in removal efficiency at pH greater than 6 might be attributed to the formation of lead hydroxide (Al-Zboon et al. 2011). In this respect, a similar behavior was shown in the studies by (Gupta et al. 2003; Al-Zboon et al. 2011).

Effect of NPCLA loading

The adsorbent dosage is recognized as an important variable since it determines the adsorbent capacity for a specified initial concentration of adsorbate. Therefore, the effect of the NPCLA dose on the removal of lead was investigated on solutions with initial lead concentrations of 30 ppm, 75 ppm, and 120 ppm at pH of 6. The removal efficiency of different doses of adsorbent (1–3 g/L) is illustrated in Fig. 8, in which the given efficiency was enhanced as the adsorbent dosage increased. As the content of the adsorbent in the aqueous medium was added, more adsorptive active sites became available and there was a rising trend in the surface area available for adsorption (Onundi et al. 2010; Hafshejani et al. 2015). In addition, a further increase in the adsorbent dose (> 2.5 g/L) did not have a great effect on the adsorption of lead ions because of the overlap in active sites at a

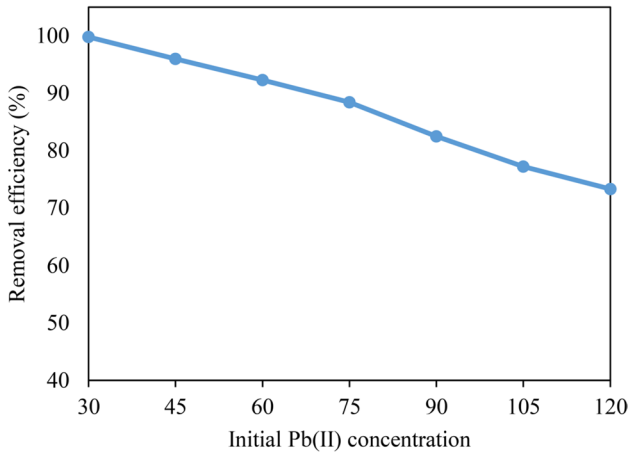

Fig. 9 Effect of the initial lead concentration (30–120 ppm) on adsorption by 1.5 g/L NPCLA at a pH of 6 and a temperature of 25 °C

higher dosage (Garg et al. 2008; Rahmani et al. 2010; Jorfi et al. 2017).

Effect of lead concentration

Figure 9 illustrates the effect that varying the initial lead concentration from 30 to 120 ppm had on the removal efficiency of the NPCLA when the dosage of NPCLA was 2.5 mg/L, the pH was 6, and the temperature was 25 °C. The figure shows that the removal efficiency decreased as the concentration of lead increased. This observation can be explained by the fact that the initial concentration of lead ions is a driving force for the transport of metal ions between the adsorbent and the solution. Furthermore, the saturation of the active binding sites prevents further uptake of ions at high concentrations of lead in solution (King et al. 2007; Garg et al. 2008; Ozdes et al. 2009).

Recyclability of adsorbent

In large-scale applications, the reusability of adsorbents is an essential factor for assessing their performance and economical aspects. In this study, six serial runs were carried out to investigate the reusability of the NPCLA at the optimum operational conditions of 30 mg/L of lead, 2.5 g/L of NPCLA, a pH of 6, and a temperature of 25 °C. Figure 10 shows the efficacy of lead degradation at each cycle. After each run, the adsorbent was separated from the mixture and treated with 0.1 M sulfuric acid to remove any lead from the surface of NPCLA. The adsorbent was then washed three times in ethanol and water, and heated in an electric oven at 90 °C for 1 day. After six runs, the NPCLA adsorbent demonstrated an outstanding stability in lead removal (Fig. 10). However, there was a slight decrease (5%) in degradation

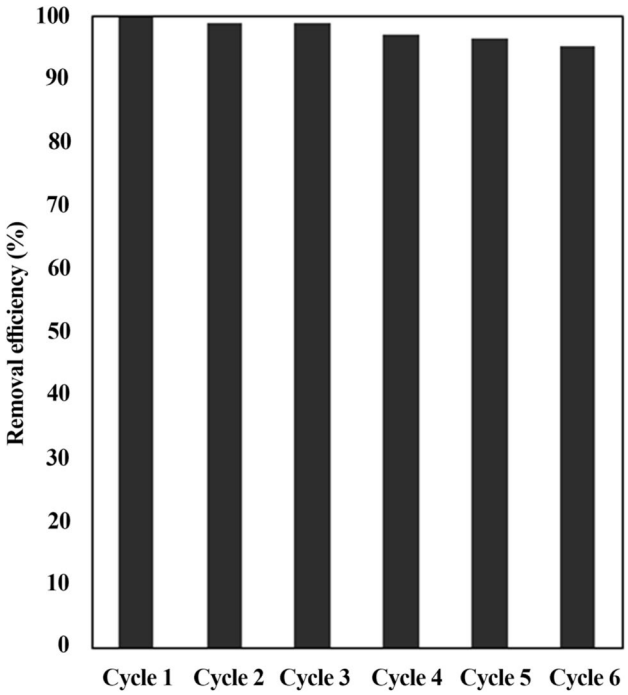

Fig. 10 Reusability of NPCLA in the lead removal process over six cycles

efficiency after six runs, which may be due to a small loss of NPCLA during the recycling and treating process and the blocking of the mesopores of the adsorbent by the lead ions and other organics, which deactivated the adsorptive sites. The results revealed that NPCLA exhibited excellent applicability, reusability, and chemical stability during the removal processes (Jorfi et al. 2017; Kumar et al. 2018).

Adsorption kinetics and isotherms

Interestingly, batch adsorption kinetics reports are useful for designing industrial columns and scale-up applications, although the experiments are usually performed in the dark and at optimum operational conditions. To investigate the adsorption character and its performance, several experiments were carried out on the kinetics and isotherms of lead on the NPCLA adsorbent. Three well-known kinetic models, the pseudo-first-order, intraparticle diffusion, and pseudo-second-order models, and two isotherm models, the Langmuir isotherm and Freundlich isotherm models, were considered for the evaluation of the experimental results. Supplementary details and constants of the kinetics, isotherms, and the corresponding regression coefficients (R^2) are represented in Table 1. As shown in the table, the correlation coefficients of the intraparticle diffusion and the pseudo-first-order models were 0.83 and 0.91, respectively, while the correlation coefficient of the pseudo-second-order model was 0.95. In other words, the results from the kinetic

Table 1 Adsorption results of lead on NPCLA

Model	Model parameters	Value
Pseudo-first order	K_1 (1/min)	0.5217
	$q_{e\,\mathrm{cal}}$ (mg/g)	0.762
	R^2	0.9156
Pseudo-second order	K_2 (g/mg.min)	3.236
	$q_{e\,\mathrm{cal}}$ (mg/g)	0.821
	R^2	0.9513
Intraparticle	K_{id} (mg/g.min$^{0.5}$)	0.011
	R^2	0.8358
Freundlich	n	4.468
	K_f (mg/g(L/mg)$^{1/n}$)	1.321
	R^2	0.8836
Langmuir	$q_{\max}$ (mg/g)	0.431
	K_L (L/mg)	1.122
	R^2	0.9893

investigation demonstrated that the pseudo-second-order kinetic model better described the behavior of the lead adsorption by the NPCLA. It is noteworthy that the pseudo-second-order model demonstrated that the chemisorption process was the dominant step in the adsorption experiment, which occurred when electrons were donated or exchanged between the lead ions and the NPCLA binding sites. Furthermore, because the R^2 value for the Langmuir isotherm model was greater than that of the Freundlich isotherm model, as shown in Table 1, the lead adsorption followed the Langmuir isotherm model. The maximum monolayer adsorption capacity ($q_{\max}$) of 0.431 for lead was calculated from the Langmuir adsorption isotherm, which demonstrated the efficient adsorption of the ions on the surface of the NPCLA. As a result, the NPCLA could be considered to be an effective adsorbent for heavy metals, such as lead (Jafari et al. 2016; Hayati et al. 2019; Moradi et al. 2019; Karimi Pasandideh et al. 2016; Ahmadi et al. 2017).

Conclusion

In this paper, a facile synthesis procedure was used to prepare NPCLA, which was used as an efficient adsorbent for the removal of lead from aqueous solutions. The adsorbent was characterized using various analyses, such as XRD, FTIR, FESEM, EDAX, EDS, and BET. The results of the BET analysis revealed that the NPCLA had a high specific surface area, while the BJH analysis demonstrated the mesoporous structure of the NPCLA. In addition, the FESEM micrographs showed that the nanoparticles had porous structures and agglomerated spherical-shaped morphology, which are effective for the adsorption process. EDS and EDAX analysis showed that the main elements in the NPCLA were O, C, Ca, and Si. The results from the removal experiments indicated that the optimum operational conditions for complete lead removal within a reaction time of 100 min at an ambient temperature were pH of 6, an NPCLA dosage of 2.5 g/L, and an initial lead concentration of 30 mg/L. The stability and reusability of the NPCLA adsorbent were investigated through six cycles. After six cycles, the adsorption efficiency decreased from 100% to 95.2%. The adsorption isotherms fitted with the Langmuir isotherm model and can be described with the pseudo-second-order kinetic model. The maximum monolayer adsorption capacity ($q_{\max}$) of 0.431 for lead was calculated from the Langmuir adsorption isotherm, which demonstrated that the surface of the NPCLA provided efficient adsorption of lead ions. In addition, the R^2 value of the Langmuir isotherm model ($R^2 = 0.9893$) was greater than that of the Freundlich isotherm model. The findings of this study revealed that the NPCLA had effectively adsorbed lead from aqueous solutions under neutral conditions.

Acknowledgements This article was supported by the Petroleum University of Technology, Abadan, Iran (Project No.: 2146-3242).

Compliance with ethical standards

Conflict of interest The authors declare no competing financial interest.

References

Ahmadi M, Hazrati Niari M, Kakavandi B (2017) Development of maghemite nanoparticles supported on cross-linked chitosan (γ-Fe_2O_3@CS) as a recoverable mesoporous magnetic composite for effective heavy metals removal. J Mol Liq. https://doi.org/10.1016/j.molliq.2017.10.014

Al-Zboon K, Al-Harahsheh MS, Hani FB (2011) Fly ash-based geopolymer for Pb removal from aqueous solution. J Hazardous Mater 188(1–3):414–421. https://doi.org/10.1016/j.jhazmat.2011.01.133

Bachari Z, Isari AA, Mahmoudi H, Moradi S, Mahvelati EH (2019) Application of natural surfactants for enhanced oil recovery–critical review. In: IOP conference series: earth and environmental science, Vol 221, issue 1. IOP Publishing, p 012039

Bhatnagar A, Sillanpää M (2010) Utilization of agro-industrial and municipal waste materials as potential adsorbents for water treatment: a review. Chem Eng J 157(2–3):277–296. https://doi.org/10.1016/j.cej.2010.01.007

Bhattacharyya KG, Sharma A (2004) Adsorption of Pb(II) from aqueous solution by *Azadirachta indica* (neem) leaf powder. J Hazard Mater 113(1–3):97–109. https://doi.org/10.1016/j.jhazmat.2004.05.034

Bux SK et al (2010) Rapid solid-state synthesis of nanostructured silicon. Chem Mater 22(8):2534–2540. https://doi.org/10.1021/cm903410s

Chakravarty S et al (2010) Removal of Pb(II) ions from aqueous solution by adsorption using bael leaves (*Aegle marmelos*). J Hazard Mater 173(1–3):502–509. https://doi.org/10.1016/j.jhazmat.2009.08.113

Dippong T et al (2017) Size and shape-controlled synthesis and characterization of $CoFe_2O_4$ nanoparticles embedded in a PVA-SiO_2 hybrid matrix. J Anal Appl Pyrolysis 128(August):121–130. https://doi.org/10.1016/j.jaap.2017.10.018

Dizadji N, Abootalebi Anaraki N (2011) Adsorption of chromium and copper in aqueous solutions using tea residue. Int J Environ Sci Technol 8(3):631–638. https://doi.org/10.1007/BF03326248

Dubey A, Shiwani S (2012) Adsorption of lead using a new green material obtained from *Portulaca* plant. Int J Environ Sci Technol 9(1):15–20. https://doi.org/10.1007/s13762-011-0012-8

El-Ashtoukhy ESZ, Amin NK, Abdelwahab O (2008) Removal of lead (II) and copper (II) from aqueous solution using pomegranate peel as a new adsorbent. Desalination 223(1–3):162–173. https://doi.org/10.1016/j.desal.2007.01.206

Eshraghi F et al (2016) Cadmium removal from aqueous solution by *Prosopis Cineraria* leaf ash abstract. Am J Oil Chem Technol 4(1):4–11

Garg A, Mittal SK (2013) Review on *Prosopis cineraria*: a potential herb of Thar desert. Drug Invent Today 5(1):60–65. https://doi.org/10.1016/j.dit.2013.03.002

Garg U et al (2008) Removal of cadmium (II) from aqueous solutions by adsorption on agricultural waste biomass. J Hazard Mater 154(1–3):1149–1157. https://doi.org/10.1016/j.jhazmat.2007.11.040

Gholipour Z et al (2012) Sturctural flexibility under oxidative coupling of methane; main chemical role of alkali ion in [Mn + (Li, Na, K or Cs) + W]/SiO_2 catalysts. Iran J Sci Technol Trans A Sci 36(2):189–211. https://doi.org/10.1126/science.1130992

Granbohm H et al (2017) Preparation and photocatalytic activity of quaternary GO/TiO_2/Ag/AgCl nanocomposites. Water Air Soil Pollut. https://doi.org/10.1007/s11270-017-3313-9

Gueu S et al (2007) Kinetics and thermodynamics study of lead adsorption on to activated carbons from coconut and seed hull of the palm tree. Int J Environ Sci Technol 4(1):11–17. https://doi.org/10.1007/BF03325956

Günay A, Arslankaya E, Tosun I (2007) Lead removal from aqueous solution by natural and pretreated clinoptilolite: adsorption equilibrium and kinetics. J Hazard Mater 146(1–2):362–371. https://doi.org/10.1016/j.jhazmat.2006.12.034

Gupta VK et al (2003) Removal of cadmium and nickel from wastewater using bagasse fly ash: a sugar industry waste. Water Res 37(16):4038–4044. https://doi.org/10.1016/S0043-1354(03)00292-6

Hafshejani LD et al (2015) Removal of zinc and lead from aqueous solution by nanostructured cedar leaf ash as biosorbent. J Mol Liq 211(December):448–456. https://doi.org/10.1016/j.molliq.2015.07.044

Hayati F et al (2018) Photocatalytic decontamination of phenol and petrochemical wastewater through ZnO/TiO_2 decorated on reduced graphene oxide nanocomposite: influential operating factors, mechanism, and electrical energy consumption. RSC Adv 8(70):40035–40053. https://doi.org/10.1039/C8RA07936F

Hayati F, Isari AA, Anvaripour B, Fattahi M, Kakavandi B (2019) Ultrasound-assisted photocatalytic degradation of sulfadiazine using MgO@ CNT heterojunction composite: effective factors, pathway and biodegradability studies. Chem Eng J 381:122636

Isari AA et al (2018) Photocatalytic degradation of rhodamine B and real textile wastewater using Fe-doped TiO_2 anchored on reduced graphene oxide (Fe-TiO_2/rGO): characterization and feasibility, mechanism and pathway studies. Appl Surf Sci 462:549–564. https://doi.org/10.1016/j.apsusc.2018.08.133

Jafari AJ et al (2016) Application of mesoporous magnetic carbon composite for reactive dyes removal: process optimization using response surface methodology. Korean J Chem Eng 33(10):2878–2890. https://doi.org/10.1007/s11814-016-0155-x

Jorfi S et al (2017) Adsorption of Cr(VI) by natural clinoptilolite zeolite from aqueous solutions: isotherms and kinetics. Pol J Chem Technol 19(3):106–114. https://doi.org/10.1515/pjct-2017-0056

Karimi Pasandideh E et al (2016) Silica-coated magnetite nanoparticles core-shell spheres (Fe_3O_4@SiO_2) for natural organic matter removal. J Environ Health Sci Eng 14(1):1–13. https://doi.org/10.1186/s40201-016-0262-y

Kaushik N, Kumar V (2003) Khejri (*Prosopis cineraria*)-based agroforestry system for arid Haryana, India. J Arid Environ 55(3):433–440. https://doi.org/10.1016/S0140-1963(02)00289-6

King P et al (2007) Removal of lead from aqueous solution using *Syzygium cumini* L.: equilibrium and kinetic studies. J Hazard Mater 142(1–2):340–347. https://doi.org/10.1016/j.jhazmat.2006.08.027

Kumar A et al (2018) Development of g-C_3N_4/TiO_2/Fe_3O_4@SiO_2 heterojunction via sol-gel route: a magnetically recyclable direct contact Z-scheme nanophotocatalyst for enhanced photocatalytic removal of ibuprofen from real sewage effluent under visible light. Chem Eng J 353:645–656. https://doi.org/10.1016/j.cej.2018.07.153

Li YH et al (2002) Lead adsorption on carbon nanotubes. Chem Phys Lett 357(May):263–266. https://doi.org/10.1016/S0009-2614(02)00502-X

Liu P, Zhang L (2007) Adsorption of dyes from aqueous solutions or suspensions with clay nano-adsorbents. Sep Purif Technol 58(1):32–39. https://doi.org/10.1016/j.seppur.2007.07.007

Malakootian M et al (2017) Phenol removal from aqueous solution by adsorption process: study of the nanoparticles performance prepared from aloe vera and mesquite (*Prosopis*) leaves. Sci Iran 24(6):3041–3053. https://doi.org/10.24200/sci.2017.4524

Manikandar RVM et al (2009) Analgesic and anti-pyretic activity of stem bark of *Prosopis cineraria* (Linn) Druce. J Pharm Res 2(4):60–62

Mondal MK (2009) Removal of Pb(II) ions from aqueous solution using activated tea waste: adsorption on a fixed-bed column. J Environ Manag 90(11):3266–3271. https://doi.org/10.1016/j.jenvman.2009.05.025

Moradi S, Isari AA, Bachari Z, Mahmoodi H (2019) Combination of a new natural surfactant and smart water injection for enhanced oil recovery in carbonate rock: Synergic impacts of active ions and natural surfactant concentration. J Pet Sci Eng 176:1–10

Nadeem M et al (2006) Sorption of lead from aqueous solution by chemically modified carbon adsorbents. J Hazard Mater 138(3):604–613. https://doi.org/10.1016/j.jhazmat.2006.05.098

Naiya TK et al (2009) The sorption of lead(II) ions on rice husk ash. J Hazard Mater 163(2–3):1254–1264. https://doi.org/10.1016/j.jhazmat.2008.07.119

Oh SY, Imagawa H, Itahara H (2014) Si-based nanocomposites derived from layered $CaSi_2$: influence of synthesis conditions on the composition and anode performance in Li ion batteries. J Mater Chem A 2(31):12501–12506. https://doi.org/10.1039/c4ta01318b

Okoye AI, Ejikeme PM, Onukwuli OD (2010) Lead removal from wastewater using fluted pumpkin seed shell activated carbon: adsorption modeling and kinetics. Int J Environ Sci Technol 7(4):793–800. https://doi.org/10.1007/BF03326188

Onundi YB et al (2010) Adsorption of copper, nickel and lead ions from synthetic semiconductor industrial wastewater by palm shell activated carbon. Int J Environ Sci Technol 7(4):751–758. https://doi.org/10.1007/BF03326184

Ozdes D et al (2009) Removal of Pb(II) ions from aqueous solution by a waste mud from copper mine industry: equilibrium, kinetic and thermodynamic study. J Hazard Mater 166(2–3):1480–1487. https://doi.org/10.1016/j.jhazmat.2008.12.073

Payan A, Isari AA, Gholizade N (2019) Catalytic decomposition of sulfamethazine antibiotic and pharmaceutical wastewater using Cu-TiO_2@ functionalized SWCNT ternary porous nanocomposite:

influential factors, mechanism, and pathway studies. Chem Eng J 361:1121–1141. https://doi.org/10.1016/j.cej.2018.12.118

Ponce-Lira B et al (2017) Lead removal from aqueous solution by basaltic scoria: adsorption equilibrium and kinetics. Int J Environ Sci Technol 14(6):1181–1196. https://doi.org/10.1007/s13762-016-1234-6

Pouretedal HR, Sadegh N (2014) Effective removal of amoxicillin, cephalexin, tetracycline and penicillin G from aqueous solutions using activated carbon nanoparticles prepared from vine wood. J Water Process Eng 1:64–73. https://doi.org/10.1016/j.jwpe.2014.03.006

Pourjaafar M (2017) M. Pourjaafar supervisors: B. Anvaripour, M. Motavassel. Petroleum University of Technology

Qaiser S, Saleemi AR, Umar M (2009) Biosorption of lead from aqueous solution by *Ficus religiosa* leaves: batch and column study. J Hazard Mater 166(2–3):998–1005. https://doi.org/10.1016/j.jhazmat.2008.12.003

Rahmani A, Mousavi HZ, Fazli M (2010) Effect of nanostructure alumina on adsorption of heavy metals. Desalination 253(1–3):94–100. https://doi.org/10.1016/j.desal.2009.11.027

Ramasamy V, Anand P, Suresh G (2017) Biomimetic synthesis and characterization of polymer template Mn @ $CaCO_3$ nanomaterials using natural carbonate sources. Int J Mater Sci 10(7):563–569

Tang S et al (2008) Effect of nano-SiO_2 on the performance of starch/polyvinyl alcohol blend films. Carbohydr Polym 72(3):521–526. https://doi.org/10.1016/j.carbpol.2007.09.019

Wang J, Chen C (2006) Biosorption of heavy metals by *Saccharomyces cerevisiae*: a review. Biotechnol Adv 24(5):427–451. https://doi.org/10.1016/j.biotechadv.2006.03.001

Wang SG et al (2007) Removal of lead(II) from aqueous solution by adsorption onto manganese oxide-coated carbon nanotubes. Sep Purif Technol 58(1):17–23. https://doi.org/10.1016/j.seppur.2007.07.006

Zamani AA et al (2013) Adsorption of lead, zinc and cadmium ions from contaminated water onto *Peganum harmala* seeds as biosorbent. Int J Environ Sci Technol 10(1):93–102. https://doi.org/10.1007/s13762-012-0107-x